0013-7227/08/$15.00/0
Printed in U.S.A.

Endocrinology 149(5):2062–2071

doi: 10.1210/en.2007-1457

The Obesity Gene, FTO, Is of Ancient Origin, Up-Regulated during Food Deprivation and Expressed in Neurons of Feeding-Related Nuclei of the Brain

Robert Fredriksson, Maria Hägglund, Pawel K. Olszewski, Olga Stephansson, Josefin A. Jacobsson, Agnieszka M. Olszewska, Allen S. Levine, Jonas Lindblom, and Helgi B. Schiöth

Department of Neuroscience (R.F., M.H., P.K.O., O.S., J.A.J., A.M.O. J.L., H.B.S.), Functional Pharmacology, Uppsala University, Biomedical Center, SE 75124 Uppsala, Sweden; and Minnesota Obesity Center (P.K.O., A.S.L.), Department of Food Science and Nutrition (A.S.L.), St. Paul, Minnesota 55108

Gene variants of the FTO (fatso) gene have recently been strongly associated with body mass index and obesity. The FTO gene is well conserved and found in a single copy in vertebrate species including fish and chicken, suggesting that the ancestor of this gene was present 450 million years ago. Surprisingly, the FTO gene is present in two species of algae but not in any other invertebrate species. This could indicate that this gene has undergone a horizontal gene transfer. Quantitative real-time PCR showed that the gene is expressed in many peripheral and central rat tissues. Detailed *in situ* hybridization analysis in the mouse brain showed abundant expression in feeding-related nuclei of the brainstem and hypothalamus, such as the nucleus of the solitary tract, area postrema, and arcuate, paraventricular, and supraoptic nuclei as well as in the bed nucleus of the stria terminalis. Colabeling showed that the FTO gene is predominantly expressed in neurons, whereas it was virtually not found in astrocytes or glia cells. The FTO was significantly up-regulated (41%) in the hypothalamus of rats after 48-h food deprivation. We also found a strong negative correlation of the FTO expression level with the expression of orexigenic galanin-like peptide, which is mainly synthesized in the arcuate nucleus. These results are consistent with the hypothesis that FTO could participate in the central control of energy homeostasis. (*Endocrinology* 149: 2062–2071, 2008)

OBESITY IS A rapidly growing international health problem. There are about one billion adults that are overweight with a body mass index (BMI) over 25, and 300 million are obese with a BMI over 30 (http://www.who.int). Today there are more people overweight than underweight. It causes costly health problems, reduces life expectancy, and is associated with stigma and discrimination, which has a major effect on the quality of life. Obesity and overweight substantially increase the risk of morbidity from hypertension, dyslipidemia, type 2 diabetes, and coronary heart disease. Obesity is also important for the development of obstructive sleep apnea and respiratory problems, gallbladder disease, osteoarthritis, and nonalcoholic fatty liver disease as well as endometrial, breast, prostate, and colon cancers.

There are several genes associated with obesity on the human obesity map (1) such as the melanocortin 4 receptor (MC4R), leptin and the leptin receptor. However, the contribution of each specific gene to obesity is low, being highest for the MC4R gene ranging from 1–6% (2). The overall inheritability of BMI is estimated to be about 50–60%. Recently, three reports have shown a strong association of a single-nucleotide polymorphism (SNP) in a gene called FTO with both childhood and adult obesity. Frayling and colleagues (3) performed a genome-wide association study for about 490,000 autosomal SNPs in a type 2 diabetes population in the United Kingdom. They found that SNP rs9939609 in the FTO gene was strongly associated with type 2 diabetes, but this allele was also strongly associated with an increased BMI. The association between this FTO SNP and type 2 diabetes was abolished by adjustment for the BMI, suggesting that it was due to the increased BMI. The association of this variant with the BMI was replicated in 13 cohorts with over 38,000 individuals. Interestingly, 16% of the adults who were homozygous for this SNP weighed about 3 kg more and had 1.67-fold increased odds of obesity. This association was observed from age 7 yr upward, and it reflects a specific increase in fat mass (3). Independently, Dina *et al.* (4) found another SNP, rs1121980, in the first intron of the FTO gene, that was strongly associated with severe (BMI $>$ 40) adult obesity with odds ratio of 1.55 in a population of French individuals of European ancestry). Further genotyping showed a similarly strong association of several SNPs in a cohort of about 900 severely obese adults and 2700 nonobese French controls. Three of the four most significantly associated SNPs (rs17817449, rs3751812, and rs1421085) are puta-

First Published Online January 24, 2008

Abbreviations: AP, Area postrema; ARC, arcuate nucleus; BMI, body mass index; BNST, bed nucleus of the stria terminalis; Ct, threshold cycle; DAPI, 4′,6′-diamidino-2-phenylindole; DEPC, diethylpyrocarbonate; DMH, dorsomedial hypothalamic nucleus; DLGN, dorsal lateral geniculate nucleus; GALP, galanin-like peptide; GFAP, glial fibrillary acidic protein; IGN, intrageniculate leaflet; MPOA, medial preoptic area; NPY, neuropeptide Y; NTS, nucleus of the solitary tract; 2OG-Fe(II), Fe(II)-dependent 2-oxyglutarate oxygenase; POMC, proopiomelanocortin; PVN, paraventricular nucleus; SCN, suprachiasmatic nucleus; SNP, single-nucleotide polymorphism; SON, supraoptic nucleus; SSC, standard saline citrate; TBS, Tris-buffered saline; tPVN, thalamic PVN; VMH, ventromedial nucleus.

***Endocrinology* is published monthly by The Endocrine Society (http://www.endo-society.org), the foremost professional society serving the endocrine community.**

tively functional, and they were found to be similar in males and females. This report also shows associations of SNPs in the FTO gene to obesity in three additional cohorts including either children or adults (4). In an additional independent study, Scuteri and colleagues (5) showed that another SNP in FTO, rs9930506, and other nearby variants are associated with BMI, hip circumference, and total body weight in a study including over 4000 Sardinians. Additional associations of the BMI and SNPs in the FTO gene were shown in both European-American and Hispanic-American cohorts in the same report.

The analysis of previous studies (5) shows that the FTO gene maps to a region where linkage to the BMI has been reported in two previous genome-wide linkage scans (LOD = 3.2) in the Framingham Heart Study (6), and LOD = 2.2 in families with white ancestry from the Family Blood Pressure Program (7). Moreover, a deletion of the chromosome region harboring the FTO gene in one single individual was shown to result in mental retardation, finger anomalies, and obesity (8). The FTO gene was originally described in the mouse with fused toes, which has deletion of at least six genes and gross developmental phenotype (9). The association with human obesity has prompted the HUGO Gene Nomenclature Committee to change the name to fat mass and obesity associated (FTO). The FTO is currently also found under the name Fatso at the National Center for Biotechnology Information (NCBI) websites.

Together these studies provide by far the most convincing evidence for a single gene variation that alters the BMI (3, 10). The association to obesity is very strong and replicable in most populations, but the mechanism by which variants in FTO lead to obesity are unknown. After submission of this manuscript, it was reported that the FTO gene encodes a 2-oxoglutarate-dependent nucleic acid demethylase (11). The functional role of the gene in association of regulation of food intake is, however, not well characterized in terms of anatomy or functional associations to the neuropeptides that play a key role in the regulation of energy homeostasis. Several molecular components of the central regulation of body weight are evolutionarily well conserved, whereas others are highly different between species (12, 13).

Here we studied the evolutionary origin of the FTO gene and examined FTO's functional importance by determining its expression in different behavioral models of energy deficit, including a study of coregulation of FTO with other feeding related genes. We also performed detailed anatomical expression charting with emphasis on the central feeding circuits.

Materials and Methods

Sequences retrieval and phylogenetic analysis

Retrieval of protein sequences. FTO sequences were identified in GenBank (http://www.ncbi.nlm.nih.gov/) using blastp (14) searches in the nonredundant (nr) database using human FTO (NP_001073901.1) as bait. This identified FTO from 15 species: *Pan troglodytes* (XP_510968), *Macaca mulatta* (XP_001092038.1), *Canis familiaris* (XP_535301.2), *Bos taurus* (NP_001091611.1), *Equus caballus* (XP_001492838), *Ovis aries* (NP_001098401), *Ratus norvegicus* (NP_001034802), *Mus musculus* (NP_036066), *Monodelphis domestica* (XP_001372283), *Xenopus laevis* (NP_001087481.1), *Xenopus tropicalis* (NP_001017273.1), *Danio rerio* (XP_001345910), *Tetraodon nigroviridis* (CAG05424.1), *Ostreococcus tauri* (CAL57236.1), and *Ostreococcus lucimarinus* (XP_001420808).

These sequences were aligned using ClustalW 1.83 (15). Sequence Hidden Markov Models (HMMs) were constructed from alignments using HMMbuild from the HMMER (16) 2.3.2 package and calibrated using HMMcalibrate. Protein datasets (peptide all collections) were downloaded from ftp://ftp.ensembl.org/pub for the following species: *Aedes aegypti* (AegL1.46), *Anopheles gambiae* (AgamP3.46), *Caenorhabditis elegans* (WB170.46), *Ciona intestinalis* (JGI2.46), *Ciona savignyi* (CSAV2.0.46), and *Drosophila melanogaster* (BDGP4.3.46). The protein datasets were searched through with the FTO sequence HMM using HMMsearch, and all hits with E value less than 10 were manually investigated.

Phylogenetic analysis. The sequences were manually edited, and exons unique for one species (most likely wrongly predicted exons from the gene prediction programs) were removed. Also, the highly variable N termini were excluded. Alignments were performed using ClustalW 1.83 (15) and manually edited to the alignment presented in Fig. 1. The alignment was bootstrapped 1000 times using SEQBOOT from the Win32 version of the Phylip 3.6 package (17). Maximum-parsimony and neighbor joining trees were calculated on the bootstrapped alignment with PROTPARS and PROTDIST/NEIGHBOR from the Win32 version of the Phylip 3.6 package. All trees were unrooted. The parsimony trees were calculated using ordinary parsimony, and the topologies were obtained using the built-in tree-search procedure. Protein distances for the neighbor joining trees were calculated using the JTT amino acid model. Majority-rule consensus trees were constructed using CONSENSE from the Phylip 3.5 package. The trees were plotted using TreeView (18) and manually edited in Canvas 8 (ACD, Systems, Miami, FL).

Quantitative real-time PCR

Animal handling and tissue isolation. Six Sprague Dawley rats (Scanbur BK AB, Solna, Sweden), four males and two females, were housed in a temperature-, light- (12 h light, 12 h dark), and humidity-controlled environment with free access to water and standard R36 food pellets (Labfor, Lactamin, Vadstena, Sweden). Dissections were performed as we have previously described (19). After 7 d, the animals were killed by decapitation 3–6 h into the light period. Blood was collected, and central and peripheral tissues (the olfactory bulb, hypothalamus, pituitary gland, pineal gland, brainstem, hindbrain (cerebellum, pons, and medulla oblongata), spinal cord, eye, adrenal gland, skeletal muscle, adipose tissue, heart, intestine, kidney, liver, lung, spleen, thymus, ovary, uterus, testis, and epididymis) were isolated from the rats. Two whole brains were dissected into eight coronal (cross) sections (~3 mm thick) using the brain matrix as schematically shown in supplemental Fig. 1 (published as supplemental data on The Endocrine Society's Journals Online web site at http://endo.endojournals.org). The remaining brains were dissected in more detail using the rat brain matrix (coronal sections). The following regions were dissected from the sections with the guidance of a rat brain atlas (20): prefrontal cortex, cortex, and hippocampus. The first section (approximately bregma 5.20–4.20 mm) was denoted prefrontal cortex. The cortex was collected from sections approximately bregma 4.20–2.70 mm and included the primary and secondary motor cortex. The hippocampus was collected from several sections and therefore comprised the hippocampus CA1–3 and the dentate gyrus. The tissues were immersed in the RNAlater solution (Ambion, Austin, TX), kept at room temperature for 1 h, and thereafter stored at −80 C until further processed.

The same animals as in Lindblom *et al.* (21) were used in this study. Briefly, 24 (eight animals per group) outbred male Sprague Dawley rats (Alab, Sollentuna, Sweden) with the initial body weight of about 225 g were randomized into three groups: control (*ad libitum* fed), food-restricted, and food-deprived animals. Animals in the control group had free access to R36 food pellets (Labfor, Lactamin), whereas the food-restricted group for 12 d received 45 ± 1% of the amount of food consumed by controls in the same time frame. During this period, the control animals gained 40 ± 1.5% in body weight, whereas the food-restricted animals lost 8 ± 0.9%. The food-deprived animals had access to food until the last 48 h of the experiment, when they were completely deprived of food. The animals were killed by decapitation between 3 and 6 h into the light period, and the brains were rapidly removed. At

FIG. 1. Amino acid sequence alignment with the FTO sequences identified. The N-terminal part of the sequences is highly variable and varies also in length from 279 (ota) to 12 (olu) amino acids and is not shown in the figure. *Gray boxes* mark fully conserved positions, and *black boxes* mark splice sites as deduced from alignments of the cDNA sequence with the genome assembly for the respective species. *Asterisks* above a conserved region indicate that this position is considered fully conserved and hence marked in *gray*, despite not being conserved in *Tetraodon*, because there is a possibility for errors in the prediction of the Tetraodon sequence in that position. Also, part of the Tetraodon sequence is replaced with X, because this sequence is lacking due to a gap in the current genome assembly. *Gray bars* above the sequence alignment indicate regions alignable with bacterial *AlkB* according to Gerken *et al.* (11). *Roman numerals* indicate the four conserved regions described in supplemental Fig. 2. Species are abbreviated as follows: human (*hsa*, *Homo sapiens*), chimpanzee (*ptg*, *Pan troglodytes*), *Maccaca* (*mml*, *Maccaca mulata*), cow (*bta*, *Bos taurus*), dog (*cfa*, *Canis familiaris*), horse (*eca*, *Equus caballus*), sheep (*oar*, *Ovis aris*), mouse (*mmu*, *Mus musculus*), rat (*rno*, *Rattus norvegicus*), opossum (*mdo*, *Monodelphis domestica*), African clawed frog (*xla*, *Xenopus laevis*), Western clawed frog (*xtr*, *Xenopus tropicalis*), *Tetraodon* (*tnv*, *Tetraodon nigroviridis*), zebrafish (*dre*, *Danio reiro*), and two species of green algae (*ota*, *O. tauri*, and *olu*, *O. lucimarinus*).

decapitation, blood was collected in EDTA-prepared tubes, spun for the preparation of plasma, which was later stored at −20 C until used for hormonal measurements (leptin, insulin, corticosterone, ACTH, ghrelin, and adiponectin). The entire hypothalamus was isolated using the brain matrix (Activational System) and the brain atlas as a guide (20). The rostral border was at the crossing of the anterior commissure (bregma approximately −0.4 mm) and the caudal border at the end of the mammillary recess of the third ventricle (bregma approximately −4.5 mm). The dissected tissue bordered dorsally to the bed nucleus of the stria terminalis (rostral part) and zona incerta (caudal part) and laterally to the substantia innominata (rostral part) and the optic tract and internal capsule (caudal part). Individual tissue samples were rapidly frozen on dry ice, immersed in RNAlater solution (Ambion, Stockholm, Sweden), kept at room temperature for approximately 1 h to allow the solution to infiltrate the tissue, and then stored at −80 C until further processed.

RNA isolation and cDNA synthesis. Individual tissue samples were homogenized by sonication in the TRIzol reagent (Invitrogen, Breda, The Netherlands) using a Branson sonifier. Chloroform was added to the homogenate, which was then centrifuged at 10,000 × *g* at 4 C for 15 min. The water phase was transferred to a new tube, and RNA was precipitated with isopropanol. The pellets were washed with 75% ethanol, air dried at room temperature, and dissolved in RNase-free water. DNA contamination was removed by treatment with DNase I (Roche Diagnostics, Uppsala, Sweden) for 4 h at 37 C, and the DNase I was thereafter inactivated by heating the samples at 75 C for 15 min. The absence of

genomic DNA was confirmed by PCR with primers for the rat and mouse RNA extractions with glyceraldehyde-3-phosphate dehydrogenase (GAPDH; NM_017008; forward TCC CTC AAG ATT GTC AGC AA, and reverse, CAC CAC CTT CTT GAT GTC ATC) on the Dnase-treated RNA. RNA concentration was determined using a Nanodrop ND-1000 Spectrophotometer (NanoDrop Technologies, Wilmington, DE). cDNA was synthesized with MMLV reverse transcriptase (General Electric, Uppsala, Sweden), using random hexamers as primers according to the manufacturer's instructions.

Real-time PCR. The cDNA for the tissue panels was analyzed in quantitative real-time PCR with a MyiQ thermal cycler (Bio-Rad Laboratories, Stockholm, Sweden). Each real-time PCR with a total volume of 20 μl contained cDNA synthesized from 25 ng total RNA, 0.25 M each primer, 20 mM Tris/HCl (pH 8.4), 50 mM KCl, 4 mM $MgCl_2$, 0.2 mM dNTP, SYBR Green (1:50,000). Real-time PCR was performed with 0.02 U/liter *Taq* DNA polymerase (Invitrogen) under the following conditions: initial denaturation for 3 min at 95 C, followed by 50 cycles of 15 sec at 95 C, 15 sec at 54–61 C (optimal annealing temperature), and 30 sec at 72 C. This was followed by 84 cycles of 10 sec at 55 C (increased by 0.5 C per cycle). All real-time PCR experiments were performed in duplicates, and the measurements where the threshold cycle (Ct) values between the duplicates had a difference of over 0.9 were repeated. A negative control for each primer pair and a positive control with 25 ng rat genomic DNA were included on each plate. For the food-restricted and food-deprived groups, RNA was extracted and converted into cDNA as described above, and quantitative real-time PCR was run as above, with the exception that six housekeeping genes were used (supplemental Table 1). The primer sequences for the rat FTO gene is also found in supplemental Table 1. Melting point curves were included after the thermocycling to confirm that only one product with the expected melting point was formed.

Data analysis and relative expression calculations. The MyiQ software version 1.04 (Bio-Rad) was used to analyze real-time PCR data and derive Ct values. Melting curves were analyzed manually for each individual sample to confirm that only one product was amplified and that it was significantly shifted compared with the melting curve for the negative control. The sample Ct values were analyzed further if the difference between those and the negative control was greater than 2; otherwise, the transcript was considered not to be expressed. LinRegPCR (22) was used to calculate PCR efficiencies for each sample. After that, Grubbs' test (GraphPad, San Diego, CA) was applied to exclude outliers and calculate average PCR efficiency for each primer pair. The δ Ct method (23) was used to transform Ct values into relative quantities with SD, and the highest expression for each primer pair was set to 1. Hereafter, the statistical analysis for tissue panels and treatment groups was conducted differently. For the tissue panels, all values in each data set were divided by the relative quantity for genomic DNA. The GeNorm software (23) was used on the two housekeeping genes to calculate normalization factors for every tissue to compensate for differences in cDNA amount. Thereafter, the normalized quantities were calculated and compared with genomic DNA, which was set to 100%. For the food-restricted and food-deprived groups, the analysis of real-time PCR data were performed as we have previously reported (21). The data were corrected for primer efficiencies and normalized as above. Differences in gene expression between groups were analyzed using ANOVA followed by Tukey's *post hoc* test on genes significantly up- or down-regulated in the ANOVA. $P < 0.05$ was used as the criterion of statistical significance for the ANOVA. Statistics were performed using Prism (GraphPad).

In situ hybridization and immunohistochemistry

Animals. Adult male wild-type Sv129 mice were anesthetized, and the brains were fixed by transcardial perfusion before being excised. For paraffin-embedded tissue sections, the brains were fixed in zinc-formalin (Richard-Allan Scientific, Kalamazoo, MI) for 18–24 h at 40 C before dehydration and paraffin infusion (Tissue-Tek vacuum infiltration processor; Miles Scientific, Naperville, IL). Sections were cut at 7 μm using a Microm 355S STS cool-cut microtome, placed on Superfrost Plus slides (Menzel-Gläser, Braunschweig, Germany), incubated at 37 C for 18–24 h and stored at 4 C. For free-floating tissue sections, the brains were cut at 50 μm using a Leica VT1000S vibratome. For details see Lagerstrom *et al.* (24).

Synthesis of RNA probes. The FTO cDNA clone (partial expressed sequence tag clone) was obtained from Invitrogen (Groningen, The Netherlands; Invitrogen clone ID 5150225) as a glycerol stock. Plasmid DNA preparation was performed using JETstar 2.0 Plasmid Purification Midi Kit/50 (Genomed, Lohne, Germany). The clone was sequenced at MWG (Ebersberg, Germany) (https://ecom.mwgdna.com) and confirmed to contain 773 bp of the 3′-untranslated region of the mouse FTO transcript. Twenty micrograms of plasmid DNA were linearized by digestion with 30 U *Spe*I (Fermentas, Vilnius, Lithuania) for 3 h. Ribo probes were synthesized using 1 μg of the template, RiboLock RNase inhibitor (Fermentas, Helsingborg, Sweden) and 40 U RNA polymerase in the presence of digoxigenin-11-UTP or fluorescein-12-UTP (Roche Diagnostics). Probes were quantified using a NanoDrop ND-1000 spectrophotometer (NanoDrop Technologies).

In situ hybridization combined with immunohistochemistry. Paraffin-embedded tissue sections were deparaffinized by incubation in X-tra Solve (Medite Histotechnik, Burgdorf, Germany) and rehydrated by successive washes in ethanol/diethylpyrocarbonate (DEPC), ending up in 100% DEPC. Sections were fixed for 10 min in 4% paraformaldehyde followed by washes in PBS before digestion for 15 min in 20 μg/ml proteinase K (Sigma-Aldrich, Stockholm, Sweden) diluted in 10 mM Tris-HCl (pH 8.0). The sections were refixed in 4% paraformaldehyde, and additional washes in PBS were performed. Acetylation treatment for 10 min in a mixture of 1.3% triethanolamine (Sigma-Aldrich), 0.2% acetic anhydride (Sigma-Aldrich), and 0.06% HCl diluted in DEPC was done, and the sections were then permeabilized in 1% Triton X-100 (Sigma-Aldrich) in PBS for 30 min. The sections were rinsed in PBS and placed in a humidified chamber [50% formamide, 5× standard saline citrate (SSC)] before preincubation for 2–5 h in hybridization buffer. Hybridization buffer consisted of 50% formamide, 20× SSC, 50× Denhardt's solution (1% Ficoll 400, 1% polyvinylpyrrolidone and 1% BSA; Sigma-Aldrich), 10 mg/ml yeast tRNA (R6750; Sigma-Aldrich), and 10 mg/ml sheared salmon sperm single-stranded DNA (Ambion, Sweden) in 0.1% DEPC. The final concentration of 1 μg probe/ml was then heat denatured in hybridization buffer and added onto the slides. The sections were covered with glass coverslips, and hybridization was performed for 16 h at 55 C. Prewarmed 5× SSC was used to remove coverslips, and the sections were incubated in prewarmed 0.2× SSC for 1 h at 55 C and for an additional 5 min at room temperature. The sections were washed in Tris-buffered saline (TBS) and placed in a humidified chamber containing TBS. Preincubation was performed in the blocking solution (1% blocking reagent; Roche Diagnostics) in TBS followed by incubation in alkaline phosphate-conjugated anti-fluorescein Fab fragments (1:5000; Roche Diagnostics) together with the primary antibody against the rabbit glial fibrillary acidic protein (GFAP; Sigma-Aldrich) diluted 1:320 in the blocking solution. The sections were incubated in the antibody solution overnight at 4 C. Sequential washes with 2 mM levamisole (GTF Fisher, Frolunda, Sweden) in TBS with 0.1% Tween 20 followed by washes with 2 mM levamisole in 100 mM NaCl, 10 mM Tris-HCl (pH 9.5), 50 mM $MgCl_2$, and 0.1% Tween 20 were performed before color development of the alkaline phosphate-labeled probe with BM Purple or Fast Red enzyme substrate (Roche Diagnostics). The sections were washed in PBS and incubated with 4′,6′-diamidino-2-phenylindole (DAPI; 1:1000; Roche Diagnostics) in DEPC for 5 min. An additional PBS rinse was performed before the sections were incubated with Alexa fluorescent secondary antibody (1:500; Invitrogen) for 2 h in the dark. After mounting in DTG mounting media with antifade [1.25 g (2.5%) DABCO (Sigma D-2522) in 45 ml glycerol and 5 ml 0.5 Tris (pH 8.6)], the sections were analyzed with the Olympus (Japan) BX61W1 microscope and the Optigrid system using the Volocity software (Improvision, Tubingen, Germany); the staining was also analyzed by confocal microscopy using the Zeiss (Oberkochen, Germany) LSM 510 META system.

In situ hybridization on free-floating sections

In situ hybridization was performed according to Lagerstrom *et al.* (24) with 500 ng/ml probe.

Ethical statement

All animal procedures were approved by the local ethical committee in Uppsala (permit C 275/4 and C 156/4) and followed the guidelines of the European Communities Council Directive (86/609/EEC).

Results

Genome searches

We searched the nonredundant (nr) protein database using protein blast at the National Center for Biotechnology Information (NCBI) (http://www.ncbi.nlm.nih.gov/) with the human FTO as bait. These searches identified 15 FTO sequences (see Figs. 1 and 2). Thirteen of these were of vertebrate origin, whereas two originated from two species of green algae, *O. tauri* and *O. lucimarinus*. We constructed a sequence Hidden Markov Model (HMM) from these sequences and searched the protein dataset of several invertebrate species: *A. aegypti*, *As gambiae*, *C. elegans*, *D. melanogaster*, *C. intestinalis*, *C. savignyi*, *Branchiostoma floridae*, and *Nematostella vectensis*. These species represent at least four distinct developmental lineages of animals, ecdysozoa (with nematoda and arthropoda), tunicates, cephalochordates, and cnidarians, and no FTO sequence could be found. We also searched the chicken genome at UCSC (http://genome.ucsc.edu/cgi-bin/hgBlat/) and identified a partial FTO sequence representing exon 1, part of exon 2, exons 3–4, and exon 6 (data not shown), although we were unable to identify the rest of the gene due to gaps in the genome assembly. In addition, we searched the 1.4× shotgun assembly of a cartilaginous fish, the elephant shark (at http://esharkgenome.imcb.a-star.edu.sg/) using translated blast with the human FTO as bait. We identified single-read sequences representing exons 2–4, 6, and 7 (not shown). These data suggest that FTO is present as a functional gene also in birds and cartilaginous fish, although we cannot fully exclude the possibility that these two sequences are pseudogenes. We did not identify FTO in prevertebrate chordates (*B. floridae* or *Ciona*), insects, *C. elegans*, *Nematostella*, yeast, or green plants. Taken together, FTO appears to be present within vertebrates, missing in invertebrate animals, fungi, and green plants, but present in algae, which split from the lineage leading to vertebrates early in eukaryotic evolution about 850 (25) to 1200 (26) million years ago.

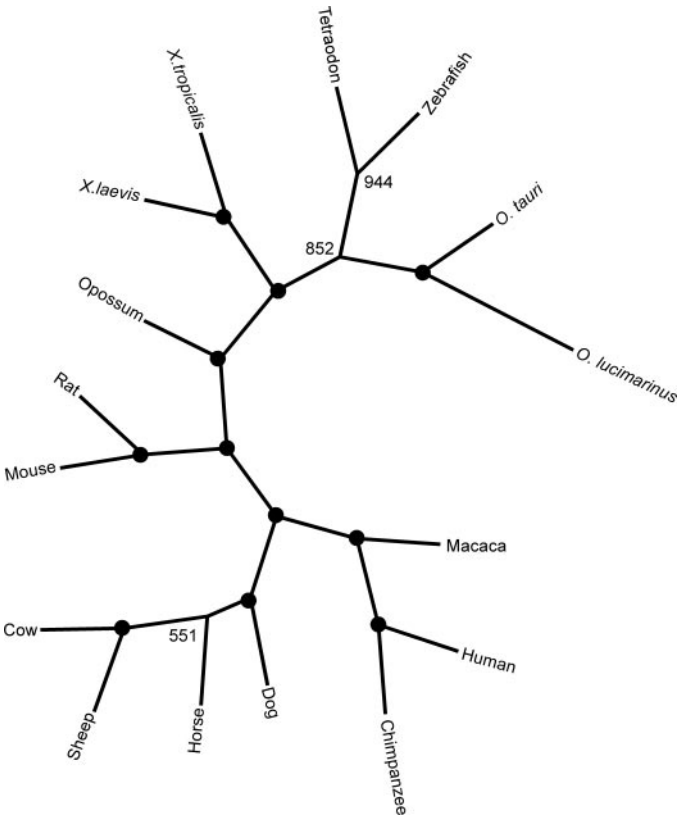

FIG. 2. Phylogenetic majority rule consensus tree showing the relationship between the FTO sequences obtained. The tree is derived from 1000 bootstrap replicas from the same alignment with the topology inferred using maximum parsimony. *Black circles* on nodes indicate 95% or higher bootstrap support, whereas *numbers* on nodes indicates actual numbers of trees in the dataset that support the node.

After submission of the first version of this manuscript, Gerken *et al.* (11) showed, using iterated PSI-BLAST searches, that FTO has remote sequence similarity as well as shared structural features with Fe(II)-dependent 2-oxyglutarate oxygenases [2OG-Fe(II)], with highest similarity to *AlkB* from *Escherichia coli*. In the same paper, it was also shown that FTO is able to catalyze the turnover of 1-methyl adenine methylated oligonucleotides, a known substrate of other 2OG-Fe(II), although FTO was unable to catalyze the turnover of other known 2OG-Fe(II) substrates. The sequence similarity between human FTO and *E. coli AlkB* is very low with only 25 of the 505 residues (4.9%) of human FTO being conserved in *E. coli AlkB*. Further sequence analyses are presented elsewhere (27, 28).

Alignment and phylogeny

The amino acid sequence alignment of the FTO sequences is shown in Fig. 1. *Gray boxes* mark conserved residues, and *black boxes* mark splice sites. As for most genes, the exon-intron pattern is largely conserved within vertebrates, but interestingly, the algae sequences are intronless. In Fig. 1, we have also marked the part of the sequence (*gray bar* above the alignment) that can be aligned with *AlkB* from bacteria (11). At the global level, it can be seen that there is a large insertion of up to 85 residues in the first exon in FTO compared with *AlkB*. Interestingly, this region is also much smaller in algae compared with vertebrates, suggesting that this region expanded relatively recently in evolution. This region also displays a relatively low degree of conservation compared with the rest of the FTO gene, suggesting it could function as a spacer rather than as a functional domain. Also, the FTO sequences are significantly longer in the C-terminal region than *AlkB*, with the region corresponding to the last three exons in FTO being unique compared with *AlkB*. In Fig. 1, we have also marked four highly conserved regions in FTO, denoted I–IV (see supplemental Fig. 2). Interestingly, one of the most highly conserved regions lies in the part of FTO that is not present in *AlkB*, suggesting that this region could provide functionality or specificity that is unique for FTO compared with *AlkB*.

We made a phylogenetic tree using the maximum parsimony method (see Fig. 2) containing the predicted protein

sequences of FTO from 16 species. The mammalian FTO sequences formed three clear clusters, one each for primates, rodents, and other mammals. The opossum sequences placed basal of the mammals as expected. The sequences from nonmammalian species formed three clusters, one for frogs, one for teleost fish, and one for the algae sequences. All the nodes separating these clusters have a bootstrap support over 95%. To investigate the evolutionary distance between the sequences, we mapped maximum likelihood branch lengths onto the maximum parsimony tree topology from Fig. 2 (cells below and to the left of the diagonal in Table 1). In Table 1, we also display pair-wise amino acid identity (nonshaded cells). We plotted the evolutionary time from humans (evolutionary time from hsa *vs.* hsa = 0) to the split of the other species, where the slope of the line represents evolutionary rate (data not shown). The evolutionary distance is proportional against evolutionary time for all animals, with the exception of *Tetraodon*, as indicated in Table 1. This shows that FTO in *Tetraodon* appears to be evolving much more rapidly than FTO in other species, or this evolutionary rate could also be due to the low-quality regions in the genomic sequence from which the *Tetraodon* sequence is derived. Interestingly, FTO in algae appears to be evolving much more slowly and is only twice that of the distance between FTO in human and fish.

Real-time tissue panel

The results of quantitative expression of the FTO gene in a wide-range tissue panel are shown in Fig. 3. The results show that the FTO gene is expressed in all tested tissue types including all brain slices encompassing the entire rat brain.

In situ hybridization and immunohistochemistry

Several feeding-related sites displayed the presence of FTO mRNA (Table 2 and Fig. 4). Among the hypothalamic regions, particularly high density of labeling was observed in the arcuate (ARC), ventromedial (VMH), and supraoptic (SON) nuclei. FTO was distributed uniformly throughout the ARC, whereas the signal seemed more pronounced in the dorsal *vs.* ventral portion of the SON. The paraventricular nucleus (PVN) also contained FTO mRNA, primarily in the medial parvocellular and medial magnocellular subdivision. Sparse FTO-expressing cells were detected in the medial preoptic area (MPOA), yet they were scattered in the entire region. In addition, FTO mRNA was seen in the dorsomedial hypothalamic nucleus (DMH) and the periventricular zone around the third ventricle (Fig. 4). The analysis of extrahypothalamic sites revealed a high level of FTO expression in all portions of the bed nucleus of the stria terminalis (BNST). FTO mRNA was detected in the brainstem, including the area postrema (AP) and nucleus of the solitary tract (NTS). This gene was present only in the caudal part of the NTS. Aside from the expression in feeding-related areas, FTO mRNA was found in selected regions involved in visual processing and circadian rhythmicity, such as the suprachiasmatic nucleus (SCN) (Table 2 and Figure 4), but also dorsal lateral geniculate nucleus (DLGN), intrageniculate leaflet (IGN) and thalamic PVN (tPVN). Positive FTO signal was also seen in the hippocampus, cortex, and medial vestibular nucleus (not shown).

CNS cell types

Figure 5 shows fluorescent *in situ* hybridization of the mouse cortex (*left*) and mouse thalamus (*right*) with FTO labeled in *red*. *Green* labels indicate immunohistochemical staining for GFAP, a marker for astrocytes and glia cells. *Blue* staining is DAPI staining for nuclear DNA and, hence, serves as a marker for all cells. It is evident that there are cells staining specifically for *green* and *blue* (*arrows* marked with *asterisks*) as well as *red* and *blue* (*unmarked arrows*), but we found only one cell that had FTO overlapping with GFAP. This indicates that FTO is exclusively neuronal, possibly with very few exceptions.

The effect of food deprivation and food restriction of FTO expression

We have earlier performed studies on gene regulation during 48 h food deprivation and 45% 12-d food restriction (see *Materials and Methods* and Ref. 21). The expression level of FTO was increased in the hypothalamus of food-deprived

TABLE 1. Pair-wise amino acid identity obtained from a multiple sequence alignment

	hsa	ptg	mml	rno	mmu	bta	oar	cfa	eca	mde	xtr	xla	dre	tnv	ota	olu
hsa		99.6	97.0	86.6	86.4	86.8	86.6	90.7	90.0	66.5	53.1	53.7	45.0	38.7	28.9	27.2
ptg	0.00		96.6	86.2	86.0	86.8	86.6	90.2	89.8	66.7	52.9	53.5	45.0	38.7	28.9	27.0
mml	0.03	0.03		86.2	85.6	86.0	85.8	89.8	89.4	66.9	52.7	53.3	44.4	39.0	28.9	27.0
rno	0.13	0.14	0.14		95.9	81.2	81.0	84.4	83.3	64.3	52.7	53.1	44.8	40.3	29.7	27.6
mmu	0.13	0.14	0.15	0.04		81.6	81.4	84.4	83.1	64.5	52.9	53.3	44.6	38.7	29.7	27.8
bta	0.14	0.14	0.15	0.21	0.20		99.8	89.8	90.0	65.8	51.8	52.5	44.6	38.7	28.5	26.8
oar	0.14	0.14	0.15	0.21	0.20	0.00		89.6	89.8	65.6	51.8	52.5	44.6	38.5	28.5	26.8
cfa	0.09	0.10	0.11	0.17	0.16	0.10	0.10		93.4	66.6	53.1	53.7	46.0	38.5	28.5	26.8
eca	0.10	0.10	0.11	0.18	0.18	0.10	0.10	0.07		67.3	52.7	53.7	45.6	38.7	29.3	27.2
mde	0.45	0.45	0.44	0.49	0.49	0.46	0.47	0.45	0.44		52.0	53.3	43.0	36.0	29.9	28.4
xtr	0.86	0.87	0.89	0.87	0.88	0.93	0.93	0.90	0.89	0.92		85.0	43.0	36.7	29.9	28.6
xla	0.83	0.83	0.86	0.84	0.84	0.90	0.90	0.87	0.86	0.86	0.16		44.4	37.8	29.3	28.1
dre	1.05	1.04	1.08	1.06	1.07	1.05	1.05	1.04	1.03	1.13	1.08	1.02		49.6	26.6	26.4
tnv	1.54	1.55	1.54	1.53	1.61	1.55	1.56	1.59	1.55	1.74	1.64	1.57	0.84		23.4	23.4
ota	2.02	2.02	2.03	1.98	2.01	2.08	2.07	2.07	1.99	2.03	2.09	2.16	1.99	2.69		71.1
olu	2.04	2.06	2.09	2.07	2.07	2.11	2.11	2.10	2.06	2.08	2.12	2.16	1.99	2.58	0.37	

Cells above and to the right of the center diagonal indicate amino acid identity, whereas *cells below and to the left* indicate maximum likelihood distances obtained as described in *Materials and Methods*.

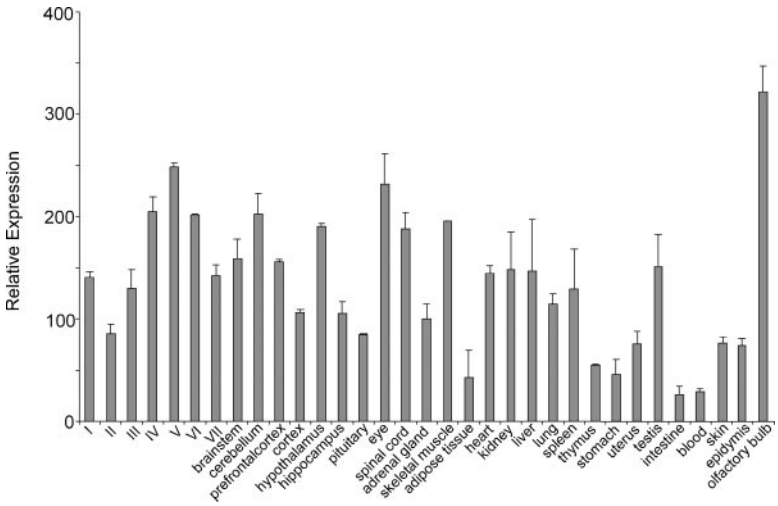

FIG. 3. Relative expression of mRNA FTO in a panel of 33 rat tissues. *Roman numerals* indicate coronal brain sections obtained with a brain matrix as illustrated in supplemental Fig. 1. All points are measured in duplicate and validated as described in *Materials and Methods*. *Error bars* indicate SD.

and food-restricted rats (n = 8 per group) by 41 and 27%, respectively (Fig. 6). Surprisingly, the effect of starvation on FTO mRNA levels in rats is opposite to that observed in mice even though a similar 48-h deprivation model was used (11). There could be several reasons for this discrepancy, but at this time, they are all speculative. It is well established that mice show much higher sensitivity to starvation compared with rats. For example, Lenaerts and colleagues (29) studied protein expression in the small intestine at several stages of food deprivation. They found that as little as a 12-h difference in the length of starvation triggers a number of differential down- and up-regulation mechanisms in mice. Another possible cause of the difference could stem from circadian rhythmicity. It should be noted that aside from the food intake network, we also found that FTO is widely expressed within the visual/circadian system, including the SCN, DLGN, IGN, and tPVN, which suggests a possible involvement in the processing of visual information (30). Noteworthy, Gerken and co-workers (11) killed the mice at the very onset of the light phase of the light-dark cycle, whereas the rats in our study were decapitated in the middle of the light phase. Because several feeding-related hypothalamic sites that express FTO, including the PVN and ARC, respond to circadian cues and receive direct projections from the SCN (31), it is possible that FTO expression in the hypothalamus can be modified by entrainment.

TABLE 2. Graded denotation of the expression of the FTO gene in the feeding circuitry involved in energy- and reward-driven consumption

Site	Expression
Nucleus accumbens	0
Ventral tegmental area	0
BNST	+++
Central nucleus of the amygdala	0
PVN	+
SON	+++
ARC	+++
Lateral hypothalamus	0
DMH	+
VMH	+++
MPOA	+
NTS	+
AP	+

Expression values were obtained from manual inspection of *in situ* hybridized mouse coronal brain sections. Scale: 0, not detectable; +, weak; ++, moderate; +++, high.

We also quantified expression levels of genes encoding for 21 hypothalamic neuropeptides: agouti-related protein (AgRP), cocaine- and amphetamine-regulated transcript (CART), CRH, dynorphin, enkephalin, galanin, galanin-like peptide (GALP), GHRH, GnRH, melanin-concentrating hormone (MCH), nociceptin/orphanin FQ, neuropeptide B, neuropeptide FF (NPFF), (NPY), orexin, oxytocin, proopio-

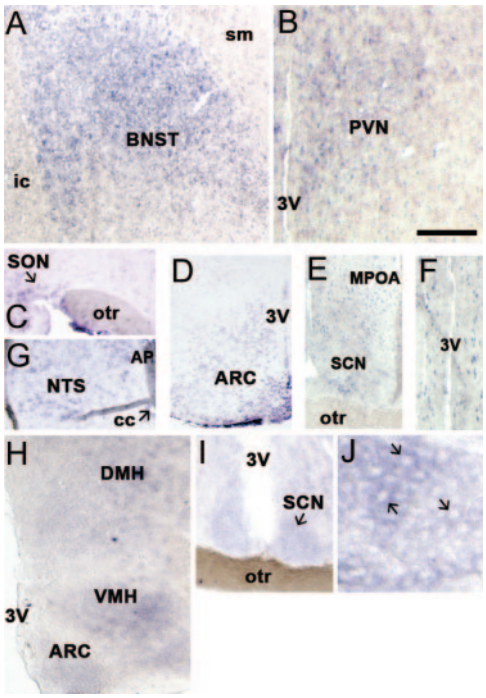

FIG. 4. FTO gene expression in feeding-related circuitry in the mouse brain. Photomicrographs depict coronal sections that have undergone the *in situ* hybridization procedure. *Scale bar*, 0.2 mm (B–G and I), 0.3 mm (A and H), and 0.05 mm (J). cc, Central canal; ic, internal capsule; otr, optic tract; sm, stria medullaris of the thalamus; 3V, third ventricle. *Arrows* in J indicate FTO mRNA-positive cellular profiles in the PVN. H, I, and J are free-floating sections, whereas all others are paraffin-embedded sections.

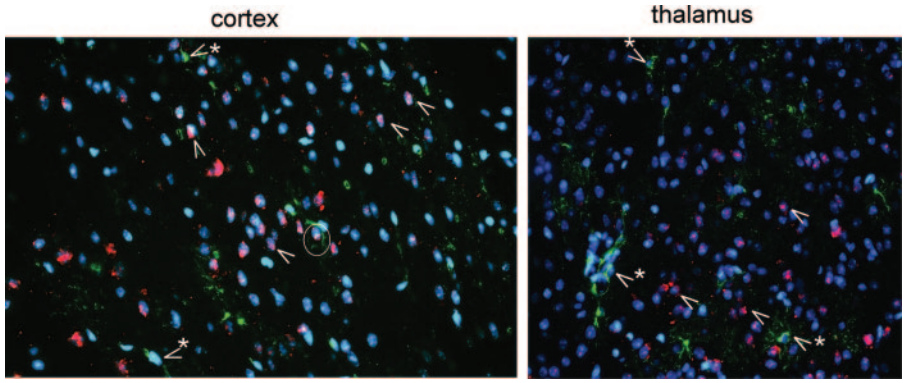

FIG. 5. Fluorescent *in situ* hybridization with the FTO probe (*red*) combined with immunohistochemistry for the astrocyte and glia cell marker GFAP (*green*). *Blue* signals are DAPI stain for cell nuclei. *White arrows* mark cells (examples) that are not colabeled with FTO and GFAP, and the *circle* marks a rare cell found to co express GFAP and FTO. Sections from four brains were hybridized and analyzed independently. As a negative control, a sense probe from the same FTO clone was used, which gave no specific hybridization signal (not shown).

melanocortin (POMC; a precursor for β-endorphin and α-MSH), prolactin-releasing peptide (PrRP), somatostatin, TRH, and vasopressin as well as circulating levels of leptin, insulin, corticosterone, ACTH, ghrelin, and adiponectin in the same rats using validated quantitative PCR and hormone measurements (Johansson, A., R. Freddriksson, S. Winnergren, M. C. Lagerstrom, A.-L. Hulting, H. B. Schioth, and J. Lindblom, submitted). This study shows, in line with large amount of literature, that plasma leptin and POMC expression are low, whereas, for example, the expression of NPY was significantly higher under both conditions as seen in Fig. 6. Here we measured the expression level of the FTO gene in the same manner in the same animals and correlated it to the expression levels of these neuropeptides and hormones. The FTO expression levels showed a strong negative correlation with expression levels of four neuropeptides. The *P* values were 0.0245, 0.0087, 0.0022, and 0.0007 against GHRH, dynorphin, galanin, and GALP, respectively. This analysis was a multivariate (all against all) of in total 28 parameters with Spearman correlations, and hence, the analysis involves 392 independent tests. If these data are corrected using the Bonferroni approach, which yields an adjusted *P* value for 5% significance of 0.00012, GALP is still borderline significant. This is accepted as a very strict correction for multiple testing for a large number of tests (32). We also identified two neuropeptides as positively correlated to FTO, TRH and NPY with *P* values of 0.01 and 0.03, respectively. Using the less strict, and possibly more appropriate method for a large number of comparisons (32), false discovery rate, expression of GALP is still significantly correlated with expression of FTO (0.03), whereas galanin is borderline significant (0.06) at the 5% confidence level.

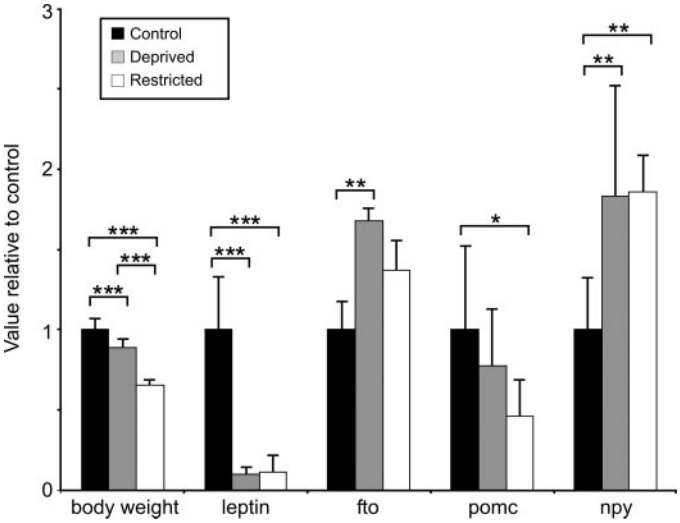

FIG. 6. Changes in expression levels of FTO, leptin, POMC, and NPY and body weight of animals [control, deprived (no food for 48 h), and restricted (45% food for 12 d)] at the last day of the experiment. The results for leptin, POMC, NPY, and body weight are taken from Johansson, A., R. Freddriksson, S. Winnergren, M. C. Lagerstrom, A.-L. Hulting, H. B. Schioth, and J. Lindblom (submitted). All data are normalized to the mean value for the control group. Significance levels were obtained from one-way ANOVA analysis followed by Tukey's *post hoc* test on datasets with $P < 0.05$ from the ANOVA. Between-group significance levels are indicated by *asterisks above the bars*: *, $P < 0.05$; **, $P < 0.01$; ***, $P < 0.001$. Each group contained eight male rats.

Discussion

The predicted 505-amino-acid-long human FTO has clear orthologs in all the fully sequenced vertebrate genomes. The presence of the FTO gene in the teleost fish suggests that this gene has been present in vertebrate evolution for at least 450 million years and is likely to be present in most vertebrates. Interestingly, FTO exists in a single copy in all of the genomes without any paralogous gene. This is also the case for the teleost genomes, which have undergone one extra round of tetraploidizations resulting in extra copies of many genes in these species. The FTO gene is not present in the prevertebrate genome of anemones (*N. vectensis*), sea squirts (tunicates), amphioxus (*Branchiostoma*), arthropods (flies), or worms (*C. elegans*). Very surprisingly, however, this gene is present in two species of algae (*O. tauri* and *O. lucimarinus*). There are three possible explanations for these findings. First, FTO could have been present in an early eukaryotic ancestor and was lost in green plants, yeast, and independently, in all four lineages of invertebrate animals. Second, the presence of FTO in green algae could be the result of a horizontal gene transfer from a vertebrate to a common ancestor of the algae genes. Third, FTO arose for the first time in a common ancestor of these two species of algae and was inserted into the vertebrate lineage by a horizontal gene transfer into a common ancestor of vertebrates before the split of cartilaginous fishes. The horizontal transfer scenarios are clearly the most parsimonious because they require only one evolutionary event, *i.e.* the transfer of the FTO gene from a vertebrate to unicellular algae or from algae to an early vertebrate. Because FTO is intronless in both species of algae and the exon-intron

structure is conserved in all vertebrate FTO sequences (Fig. 1), we suggest that the most likely scenario is that the gene was transferred from a vertebrate, perhaps a fish, to the algae via an mRNA intermediate. It is hard to date these events. but because FTO is not present in land plants (rice and *Arabidopsis*), this transfer probably occurred after the divergence of green plants from algae, approximately 480 million years ago (33). From the identification of FTO in vertebrates, we know it was present at least before the split of sharks from the lineage leading to mammals but most likely not before the split of amphioxus from the lineage leading to mammals.

The overall sequence is well conserved with 45% amino acid identity between human and zebrafish, the most distant vertebrate orthologs to the human FTO (Table 1). Figure 1 and supplemental Fig. 2 show that there are four regions within the FTO gene that are particularly well conserved. These are likely to be part of the most important functional domains of the gene. Three of these are homologs to the ALK gene (11), whereas the fourth is unique to FTO. It is interesting that three of these four regions, including the one unique to FTO, are also highly conserved in the algae sequences (see further analysis in the legend to supplemental Fig. 3).

The whole-body tissue panel shows that the FTO gene has wide-ranging expression in both peripheral and central tissues in the rat, which is in line with what was reported earlier for human tissues (3, 11). This study confirms that in rodents, FTO is widely expressed in the periphery and in the brain and enriches the previous findings in the mouse by adding twice as many tissue types in the analysis. Similar to Gerken *et al.* (11), we detected this gene in the cortex, hypothalamus, and cerebellum; however, we also found it in other central areas, including the brainstem, olfactory bulbs, pituitary, hippocampus, and prefrontal cortex. Our *in situ* data complement the real-time PCR results and show that within the hindbrain, FTO mRNA is particularly abundant in the NTS and AP, which integrate a plethora of peripheral and central signals. In the forebrain, FTO is present in discrete areas implicated in the regulation of hunger- and reward-driven consummatory responses. The comparison between the rat and mouse tissue panels presented herein and in the study by Gerken and colleagues (11) does not reveal significant species-related discrepancies. The differences are rather associated with the amount of mRNA detected in various tissue types relative to each other. We observed high FTO expression in the brain; however, some peripheral organs, such as the eye and skeletal muscle, displayed equally high levels of FTO mRNA content.

Here we focused particularly on the central circuitry associated with the regulation of food intake. Our *in situ* expression data suggest that FTO's presumed involvement in body weight control could stem from its activity within nuclei that govern feeding. FTO appears to be expressed in several brain areas within this network, and it is particularly abundant in specific nuclei of the brainstem and hypothalamic structures, such as the NTS, AP, ARC, DMH, VMH, PVN, and SON, which are the relay stations integrating both central and peripheral information pertaining to food intake. The AP, NTS, PVN, and SON respond to peripheral signals, such as changes in plasma osmolality, presence of toxins, or the level of stomach distension, whereas the ARC receives stomach ghrelin input and adipose tissue-derived leptin signals (34–36). FTO-positive cells in the vicinity of the third ventricle are likely capable of integrating peptidergic information mediated via the cerebrospinal fluid. The NTS hosts vagal afferents and transmits vagally mediated input to, among others, the PVN, SON, and ARC (30, 35, 36). The forebrain sites are reciprocally connected with each other and with the brainstem, forming a complex network. The double labeling showed that the FTO gene is predominantly expressed in neurons, whereas it is in principal absent in astrocytes or glia cells. Taken together, the data show an expression pattern that suggests that this gene could have a very specific role in the neuronal network regulating feeding.

These neuroanatomical data do not, however, allow one to link FTO with any particular aspect of feeding, such as hunger, satiety, preference, or aversion. Noteworthy, FTO mRNA is present not only in brain regions that are thought of as important for energy balance but also in regions thought of as reward related. Although the role of hypothalamic and brainstem sites seems to be associated to a large extent with maintaining the proper energy balance, the BNST, as part of the extended amygdala, affects rewarding aspects of consumption. One should note, however, that the distinction between sites influencing consumption for reward *vs.* energy is an oversimplification, because they tend to contain peptides and/or receptors involved in both types of ingestive behavior. Moreover, several of the sites where we find the FTO expression contain both anorexigenic and orexigenic peptides, such as ARC neurons that synthesize α-MSH and CART to inhibit feeding as well as agout-related peptide (AgRP), β-endorphin, and NPY, which are hyperphagic (36).

The fact that FTO expression was significantly up-regulated in the hypothalamus of rats during 48 h of food deprivation provides further support that this gene could have a regulatory role in the central feeding circuits. Moreover, FTO expression levels showed correlation with some feeding-related genes that are present within the same brain circuitry as FTO itself, with strong correlation with GALP. The other correlations of NPY, galanin, dynorphin, GHRH, and TRH were not significant considering a strict accounting for multiple testing but provide clues for further studies. These peptides all participate in food intake regulation and may have overlapping expression with the FTO gene (see *in situ* data), and it is possible that they could also follow a specific pattern of expression dependent on the level of adiposity.

Although we have focused on the main food intake circuits in this study, we also show that the FTO gene has a specific expression pattern in other parts of the brain. For example, we find consistent expression within the visual/circadian system circuitry, including the SCN, DLGN, IGN, and tPVN, which suggests a possible involvement in the processing of visual information at the central level (36). There is also abundant presence of FTO in the hippocampus and cortex, and hence, it is likely that FTO, similar to many central nervous system genes, displays a pleiotropic character influencing several systems.

In summary, we have shown that an ancestor of the FTO gene was present at least 450 million yr ago. The FTO is likely

to be present in most vertebrate species in a single copy. This gene is expressed in many tissues including the central nervous system and its feeding circuitry, where it is found in distinct nuclei of the hypothalamus, brainstem, and extended amygdala. FTO seems to be specific for neuronal cell populations. Expression of this gene is up-regulated during starvation, and it is correlated to the orexigenic peptide GALP, which is mainly expressed in the ARC. This study provides evidence supporting the central role of the FTO gene in the regulation of energy homeostasis, although it is clear that the widespread expression of FTO strongly indicates this gene's involvement in other functions as well.

Acknowledgments

Received October 23, 2007. Accepted January 14, 2008.

Address all correspondence and requests for reprints to: Robert Fredriksson, Department of Neuroscience, Biomedical Center, Box 593, SE 75124 Uppsala, Sweden. E-mail: robert.fredriksson@bmc.uu.se.

The studies were supported by Vetenskapsrådet medicine (The Swedish Research Council), AFA Insurance, Svenska Läkaresällskapet, Åhlens Foundation, The Novo Nordisk Foundation, Swedish Royal Academy of Sciences, Langmanska Kulturstiftelsen, and Magnus Bergvall Foundation. R.F. was supported by the Swedish Brain Research Foundation.

Disclosure Statement: The authors have nothing to disclose.

References

1. **Rankinen T, Zuberi A, Chagnon YC, Weisnagel SJ, Argyropoulos G, Walts B, Perusse L, Bouchard C** 2006 The human obesity gene map: the 2005 update. Obesity (Silver Spring) 14:529–644
2. **Lubrano-Berthelier C, Cavazos M, Dubern B, Shapiro A, Stunff CL, Zhang S, Picart F, Govaerts C, Froguel P, Bougneres P, Clement K, Vaisse C** 2003 Molecular genetics of human obesity-associated MC4R mutations. Ann NY Acad Sci 994:49–57
3. **Frayling TM, Timpson NJ, Weedon MN, Zeggini E, Freathy RM, Lindgren CM, Perry JR, Elliott KS, Lango H, Rayner NW, Shields B, Harries LW, Barrett JC, Ellard S, Groves CJ, Knight B, Patch AM, Ness AR, Ebrahim S, Lawlor DA, Ring SM, Ben-Shlomo Y, Jarvelin MR, Sovio U, Bennett AJ, Melzer D, Ferrucci L, Loos RJ, Barroso I, Wareham NJ, Karpe F, Owen KR, Cardon LR, Walker M, Hitman GA, Palmer CN, Doney AS, Morris AD, Smith GD, Hattersley AT, McCarthy MI** 2007 A common variant in the FTO gene is associated with body mass index and predisposes to childhood and adult obesity. Science 316:889–894
4. **Dina C, Meyre D, Gallina S, Durand E, Korner A, Jacobson P, Carlsson LM, Kiess W, Vatin V, Lecoeur C, Delplanque J, Vaillant E, Pattou F, Ruiz J, Weill J, Levy-Marchal C, Horber F, Potoczna N, Hercberg S, Le Stunff C, Bougneres P, Kovacs P, Marre M, Balkau B, Cauchi S, Chevre JC, Froguel P** 2007 Variation in FTO contributes to childhood obesity and severe adult obesity. Nat Genet 39:724–726
5. **Scuteri A, Sanna S, Chen WM, Uda M, Albai G, Strait J, Najjar S, Nagaraja R, Orru M, Usala G, Dei M, Lai S, Maschio A, Busonero F, Mulas A, Ehret GB, Fink AA, Weder AB, Cooper RS, Galan P, Chakravarti A, Schlessinger D, Cao A, Lakatta E, Abecasis GR** 2007 Genome-wide association scan shows genetic variants in the FTO gene are associated with obesity-related traits. PLoS Genet 3:e115
6. **Geller F, Dempfle A, Gorg T** 2003 Genome scan for body mass index and height in the Framingham Heart Study. BMC Genet 4(Suppl 1):S91
7. **Wu X, Cooper RS, Borecki I, Hanis C, Bray M, Lewis CE, Zhu X, Kan D, Luke A, Curb D** 2002 A combined analysis of genomewide linkage scans for body mass index from the National Heart, Lung, and Blood Institute Family Blood Pressure Program. Am J Hum Genet 70:1247–1256
8. **Stratakis CA, Lafferty A, Taymans SE, Gafni RI, Meck JM, Blancato J** 2000 Anisomastia associated with interstitial duplication of chromosome 16, mental retardation, obesity, dysmorphic facies, and digital anomalies: molecular mapping of a new syndrome by fluorescent in situ hybridization and microsatellites to 16q13 (D16S419–D16S503). J Clin Endocrinol Metab 85:3396–3401
9. **van der Hoeven F, Schimmang T, Volkmann A, Mattei MG, Kyewski B, Ruther U** 1994 Programmed cell death is affected in the novel mouse mutant Fused toes (Ft). Development 120:2601–2607
10. **Groop L** 2007 From fused toes in mice to human obesity. Nat Genet 39:706–707
11. **Gerken T, Girard CA, Tung YC, Webby CJ, Saudek V, Hewitson KS, Yeo GS, McDonough MA, Cunliffe S, McNeill LA, Galvanovskis J, Rorsman P, Robins P, Prieur X, Coll AP, Ma M, Jovanovic Z, Farooqi IS, Sedgwick B, Barroso I, Lindahl T, Ponting CP, Ashcroft FM, O'Rahilly S, Schofield CJ** 2007 The obesity-associated FTO gene encodes a 2-oxoglutarate-dependent nucleic acid demethylase. Science 318:1469–1472
12. **Cerda-Reverter JM, Peter RE** 2003 Endogenous melanocortin antagonist in fish: structure, brain mapping, and regulation by fasting of the goldfish agouti-related protein gene. Endocrinology 144:4552–4561
13. **Conlon JM, Larhammar D** 2005 The evolution of neuroendocrine peptides. Gen Comp Endocrinol 142:53–59
14. **Altschul SF, Madden TL, Schaffer AA, Zhang J, Zhang Z, Miller W, Lipman DJ** 1997 Gapped BLAST and PSI-BLAST: a new generation of protein database search programs. Nucleic Acids Res 25:3389–3402
15. **Thompson JD, Higgins DG, Gibson TJ** 1994 CLUSTAL W: improving the sensitivity of progressive multiple sequence alignment through sequence weighting, position-specific gap penalties and weight matrix choice. Nucleic Acids Res 22:4673–4680
16. **Eddy SR** 1998 Profile hidden Markov models. Bioinformatics 14:755–763
17. **Felsenstein J** 1993 Software manual distributed by the author. Department of Genetics, University of Washington, Seattle (see http://evolution.genetics.washington.edu/phylip/faq.html#citation)
18. **Page RD** 1996 TreeView: An application to display phylogenetic trees on personal computers. Comput Appl Biosci 12:357–358
19. **Roman E, Ploj K, Gustafsson L, Meyerson BJ, Nylander I** 2006 Variations in opioid peptide levels during the estrous cycle in Sprague-Dawley rats. Neuropeptides 40:195–206
20. **Paxinos G, Franklin KB** 2001 The mouse brain in stereotaxic coordinates. 2nd ed. San Diego: Academic Press
21. **Lindblom J, Johansson A, Holmgren A, Grandin E, Nedergard C, Fredriksson R, Schioth HB** 2006 Increased mRNA levels of tyrosine hydroxylase and dopamine transporter in the VTA of male rats after chronic food restriction. Eur J Neurosci 23:180–186
22. **Ramakers C, Ruijter JM, Deprez RH, Moorman AF** 2003 Assumption-free analysis of quantitative real-time polymerase chain reaction (PCR) data. Neurosci Lett 339:62–66
23. **Vandesompele J, De Preter K, Pattyn F, Poppe B, Van Roy N, De Paepe A, Speleman F** 2002 Accurate normalization of real-time quantitative RT-PCR data by geometric averaging of multiple internal control genes. Genome Biol 3:RESEARCH0034
24. **Lagerstrom MC, Rabe N, Haitina T, Kalnina I, Hellstrom AR, Klovins J, Kullander K, Schioth HB** 2007 The evolutionary history and tissue mapping of GPR123: specific CNS expression pattern predominantly in thalamic nuclei and regions containing large pyramidal cells. J Neurochem 100:1129–1142
25. **Cavalier-Smith T** 2002 The phagotrophic origin of eukaryotes and phylogenetic classification of Protozoa. Int J Syst Evol Microbiol 52:297–354
26. **Wang DY, Kumar S, Hedges SB** 1999 Divergence time estimates for the early history of animal phyla and the origin of plants, animals and fungi. Proc Biol Sci 266:163–171
27. **Robbens S, Rouze P, Cock JM, Spring J, Worden AZ, Van de Peer Y** 2007 The FTO gene, implicated in human obesity, is found only in vertebrates and marine algae. J Mol Evol 66:80–84
28. **Sanchez-Pulido L, Andrade-Navarro MA** 2007 The FTO (fat mass and obesity associated) gene codes for a novel member of the non-heme dioxygenase superfamily. BMC Biochem 8:23
29. **Lenaerts K, Sokolovic M, Bouwman FG, Lamers WH, Mariman EC, Renes J** 2006 Starvation induces phase-specific changes in the proteome of mouse small intestine. J Proteome Res 5:2113–2122
30. **Horowitz SS, Blanchard JH, Morin LP** 2004 Intergeniculate leaflet and ventral lateral geniculate nucleus afferent connections: an anatomical substrate for functional input from the vestibulo-visuomotor system. J Comp Neurol 474:227–245
31. **Escobar C, Martinez-Merlos MT, Angeles-Castellanos M, Del Carmen Minana M, Buijs RM** 2007 Unpredictable feeding schedules unmask a system for daily resetting of behavioural and metabolic food entrainment. Eur J Neurosci 26:2804–2814
32. **Liu P, Hwang JT** 2007 Quick calculation for sample size while controlling false discovery rate with application to microarray analysis. Bioinformatics 23:739–746
33. **Qiu YL, Palmer JD** 1999 Phylogeny of early land plants: insights from genes and genomes. Trends Plant Sci 4:26–30
34. **Fry M, Ferguson AV** 2007 The sensory circumventricular organs: brain targets for circulating signals controlling ingestive behavior. Physiol Behav 91:413–423
35. **Horvath TL** 2005 The hardship of obesity: a soft-wired hypothalamus. Nat Neurosci 8:561–565
36. **Horvath TL, Diano S, Tschop M** 2004 Brain circuits regulating energy homeostasis. Neuroscientist 10:235–246